LUND UNIVERSITY

GaAsP Nanowires Grown by Aerotaxy

Metaferia, Wondwosen; Persson, Axel R.; Mergenthaler, Kilian; Yang, Fangfang; Zhang, Wei; Yartsev, Arkady; Wallenberg, Reine; Pistol, Mats Erik; Deppert, Knut; Samuelson, Lars; Magnusson, Martin H.

GaAsP Nanowires Grown by Aerotaxy

Wondwosen Metaferia,*[†,‡] Axel R. Persson,[†,§] Kilian Mergenthaler,[†,‡] Fangfang Yang,[†,‡] Wei Zhang,[†,∥] Arkady Yartsev,[†,∥] Reine Wallenberg,[†,§] Mats-Erik Pistol,[†,‡] Knut Deppert,[†,‡] Lars Samuelson,[†,‡] and Martin H. Magnusson*[†,‡]

[†]NanoLund and [‡]Solid State Physics, Lund University, Box 118, SE-22100 Lund, Sweden

[§]nCHREM/Centre for Analysis and Synthesis and [∥]Chemical Physics, Lund University, Box 124, SE-22100 Lund, Sweden

S Supporting Information

ABSTRACT: We have grown GaAsP nanowires with high optical and structural quality by Aerotaxy, a new continuous gas phase mass production process to grow III−V semiconductor based nanowires. By varying the PH_3/AsH_3 ratio and growth temperature, size selected $GaAs_{1−x}P_x$ nanowires (80 nm diameter) with pure zinc-blende structure and with direct band gap energies ranging from 1.42 to 1.90 eV (at 300 K), (i.e., $0 \leq x \leq 0.43$) were grown, which is the energy range needed for creating tandem III−V solar cells on silicon. The phosphorus content in the NWs is shown to be controlled by both growth temperature and input gas phase ratio. The distribution of P in the wires is uniform over the length of the wires and among the wires. This proves the feasibility of growing GaAsP nanowires by Aerotaxy and results indicate that it is a generic process that can be applied to the growth of other III−V semiconductor based ternary nanowires.

KEYWORDS: GaAsP nanowires, zincblende, gas phase, Aerotaxy
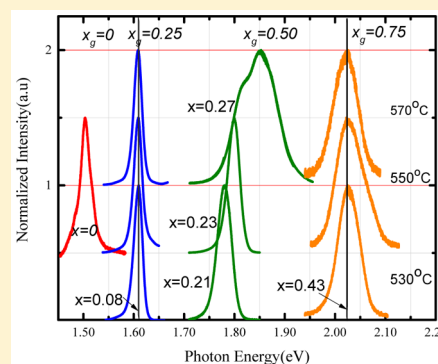
The III−V nanowires exhibit several interesting properties, such as controlled dimensions and high aspect ratio, high carrier mobility, and wide energy band gap tunability, making them excellent building blocks for future electronic, photonic, and photovoltaic devices. So far, remarkable progress has been made from understanding of fundamental physics of one-dimensional (1D) systems of NWs[1] to the demonstration of working nanowire electro-optic devices, such as light-emitting diodes,[2] high-efficiency solar cells,[3,4] ultralow threshold lasers,[5] and memory devices.[6] Previous works[7,8] have addressed fabrication issues of device quality binary and ternary III−V nanowires and nanowire heterostructures. However, commerci-alization of nanowire-based devices is, among other factors, limited by the lack of cost-effective, large-scale production processes with high degree of control of wire dimensions, crystallinity, and material composition. The common method to produce nanowires is epitaxy in different techniques such as in metal organic vapor phase epitaxy (MOVPE),[9−11] molecular beam epitaxy (MBE)[12] and chemical beam epitaxy (CBE),[13] which are all slow and batch-based. It has been shown that regardless of the techniques, epitaxy has been effective in terms of structural, electrical, and optical qualities and material compositions of nanowires. Nevertheless, low growth rate, high cost, small size, and availability of III−V substrates limit the commercial development of epitaxial growth of nanowires. Therefore, the low cost, efficient, continuous, and scalable gas phase process called Aerotaxy has been developed[14] by which GaAs nanowires have been grown with controlled size, doping, and crystal structure.[14,15]

In Aerotaxy, aerosol-synthesized and size-selected catalyst nanoparticles (typically Au), transported by a N_2 carrier gas, are mixed with traditional MOVPE precursors in a flow-through reactor at atmospheric pressure. Nanowires are produced continuously in the process in large numbers and with growth rates up to 3 orders of magnitude higher than substrate-based nanowire growth in MOVPE. Unlike in epitaxial growth of thin films, where rapid growth rates are associated with poor quality material, a high growth rate for III−V nanowires has been shown to improve the material quality substantially and also resulted in untapered wires with uniform diameter over considerable length.[16] Therefore, with further advancement in the equipment design and optimal growth conditions Aerotaxy could solve both cost and material quality issues of III−V nanowires for future optoelectronic and other device applications.

Here, we present growth of GaAsP nanowires using the Aerotaxy process. Specifically, we show wires with $E_g \sim 1.7$ eV, which is optimal for making nanowire-based tandem photo-voltaics with silicon as the lower-energy cell. The wide tunability of the energy band gap from near-infrared ($E_g = 1.42$ eV) to visible regions ($E_g = 2.3$ eV), makes GaAsP an important ternary alloy also for other optoelectronic applications. One challenge in the growth of ternary III−V semiconductors such as GaAsP is the different decomposition

rate of group-V precursors[17] (AsH$_3$ and PH$_3$ in this case) resulting in unequal vapor–solid distribution of As or P in the grown material, which in turn may result in difficulties to control the overall composition. The use of Au catalysts for the NW growth further complicates this phenomenon as it influences the hydride decomposition and hence the incorporation of the species.[17] By using X-ray energy dispersive spectroscopy (XEDS) in the transmission electron microscope (TEM) and photoluminescence (PL), the P content and hence the band gap of the resulting GaAsP NWs was obtained and is discussed in relation to the growth parameters. The optical and structural quality of the NWs were evaluated by both low-temperature and room-temperature PL, time-resolved PL, and transmission electron microscopy (TEM). Incorporation rates of P with respect to As atoms in the nanowires were estimated and the vapor-to-solid distribution determined.

The growth of NWs in Aerotaxy involves two major process stages. The first stage is production of size-selected Au nanoparticles (NPs) in an aerosol system as described by Magnusson et al.,[18] where the aerosol is formed by evaporating metallic Au at ~1800 °C in a tube furnace ("HT" in Figure 1).
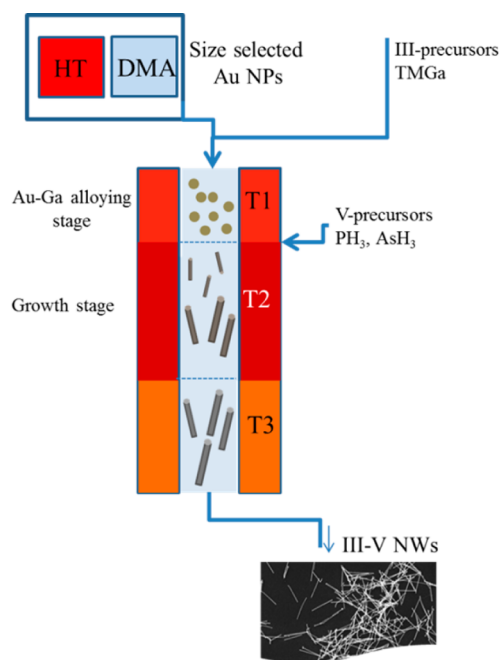
Figure 1. Schematic of the Aerotaxy system used here (not to scale). Size-selected Au particles and group III precursor flows are introduced by an inlet at the top in the first stage of the reactor and group V sources are introduced in the second stage from the side. Nanowire growth starts at this stage. The growth temperature is controlled in the middle zone (T2) and the other two temperature zones T1 and T3 are designed to balance and control the temperature profile. The nanowires are collected on a silicon substrate in an electrostatic precipitator.

The vapor is carried out of the furnace by a continuous flow of N$_2$ at 1.5 L/min, and upon cooling nanoparticle aggregates of various shapes and sizes are formed. The particles are reshaped into compact spheres in a sintering tube furnace at 550 °C, and a differential mobility analyzer (DMA)[19] is then used for size selection, typically set to 80 nm in diameter. The size-selected Au nanoparticles are then transported to the flow-through reactor for the second process stage: Au catalyst mediated III–

V nanowire growth. The group III precursor, trimethylgallium (TMGa), is added to the aerosol of Au nanoparticles and preheated to 430 °C to form a Ga–Au alloy in the first temperature (T1) zone of the reactor. The group V precursors (AsH$_3$ and PH$_3$) are added to the aerosol in the second temperature (T2) zone, the temperature of which was varied between 530 and 570 °C, while the third zone temperature (T3) was fixed at 130 °C (needed to keep the T2 temperature profile stable). T1 and T3 were fixed for all experiments. Downstream the Aerotaxy reactor, the nanowire product can be collected on any substrate (e.g., Si (used in this case), quartz, TEM grids, plastic) in an electrostatic precipitator with a collection voltage of 10 kV, equipped with a pump/purge system and placed inside a glovebox. Figure 1 shows a simplified schematic of the aerosol based Aerotaxy system used in this work.

By varying the growth temperature (T2) and the PH$_3$ and AsH$_3$ flows, experiments were designed to study the effect of these growth parameters on the resulting GaAsP NWs in terms of energy band gap, optical, and structural qualities. The NW sample collection time was 5 min for all experiments. Note that the sampling time has no relevance in terms of any of the NW properties apart from the amount of wires that can be collected, that is, longer collection time results only in a higher NW density on the substrate. This makes Aerotaxy a continuous mass production process for NWs.

Scanning electron microscopy (SEM) was used to study the morphology of the NWs, and from which the length of the NWs was measured. The structural quality of the wires was investigated by a Jeol 3000F TEM, operating at 300 kV. For compositional analysis, energy dispersive X-ray spectroscopy (in the TEM) and low-temperature PL were used. For PL measurements, the samples were excited with a frequency doubled solid state laser emitting at 532 nm, focused on the sample with a resulting excitation power density of approximately 400 W/cm^2. The ensemble PL signal originates from tens to hundreds of NWs, depending on random local variations on the sample, cf. Figure 2. The samples were kept in a liquid helium flow cryostat at 4 K. In addition, low-temperature (78 K) time-resolved PL spectroscopy was performed using a pulsed (100 fs pulses at 80 MHz) Ti:sapphire laser emitting at 800 nm to study the carrier recombination processes in the NWs.

The growth of GaAsP NWs in Aerotaxy initiates from the size-selected (80 nm) Au particles synthesized by the aerosol system. In substrate-based NW growth methods, the growth starts by formation of Au–Ga alloyed nanoparticles and subsequently new atomic planes preferentially nucleate by forming a crystal substrate–nanoparticle–vapor triple phase boundary.[20] In Aerotaxy, however, the substrate–nanoparticle interface does not exist, at least not initially. Instead, we have proposed that the preferential nucleation of new atomic planes takes place on the III–V (111)-crystalline facet that forms first on the Au–Ga surface.[14]

Figure 2a–d show SEM images (see also Supporting Information, S1) of GaAsP NWs grown at 550 °C and with different group V gas phase ratio $\frac{[PH_3]}{[PH_3]+[AsH_3]} = X_g = 0.00$, 0.25, 0.50, and 0.75, respectively, while using the same TMGa flow with molar fraction of 2.8×10^{-4} in all cases. The molar fraction of the V source was 2.3×10^{-4} for $X_g = 0.00$, 0.25, and 0.50 that resulted in a V/III ratio of 0.82, whereas for $X_g = 0.75$ the V/III was set to 1.64. The length of the nanowires was
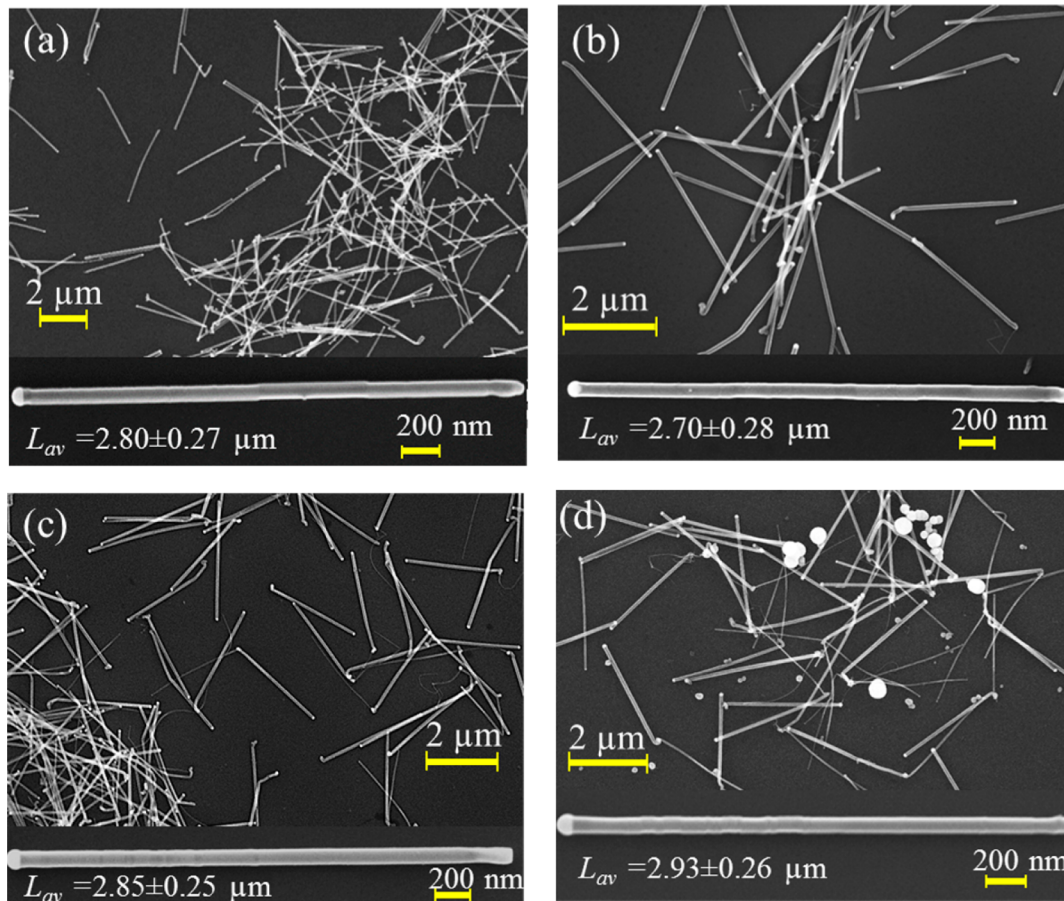
Figure 2. SEM images of GaAs$_{(1-x)}$P$_x$ NWs grown at 550 °C and X_g of (a) 0.00, pure GaAs (b) 0.25, (c) 0.50, and (d) 0.75. L_{av} represents the average NW length with the ± fractions representing 1 standard deviation based on 30 measured wires. The lower panel in each image is a representative single NW image.
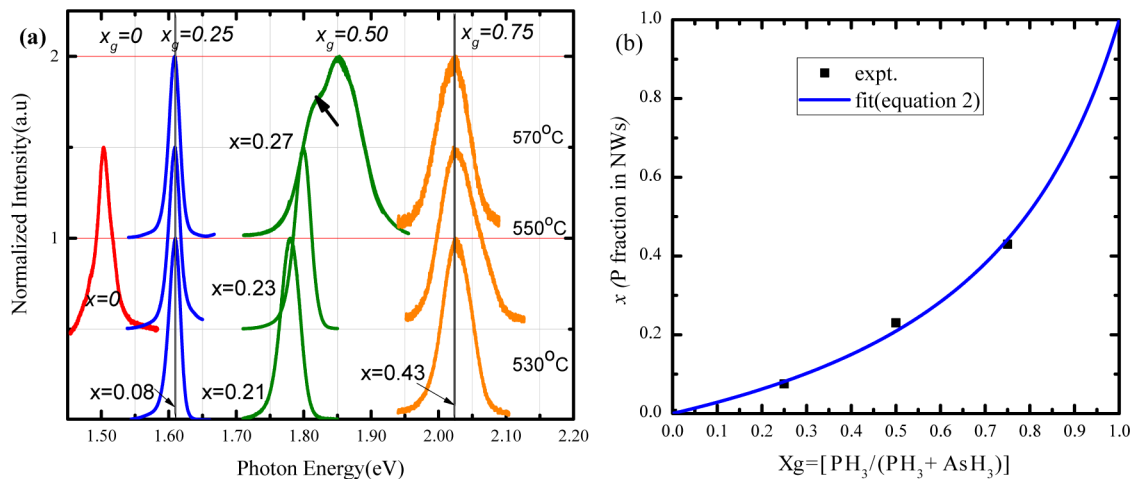

Figure 3. (a) Low-temperature photoluminescence spectra from GaAsP NWs grown with different PH$_3$ (X_g = 0.25, 0.50, and 0.75) gas phase ratios and at three different temperatures (530, 550, and 570 °C); the arrow indicates a shoulder at 1.81 eV, the origin of which is not known at present. The spectrum from intrinsic GaAs (X_g = 0) NWs grown at 550 °C is included as a reference. (b) A plot showing extracted solid phase ratio versus input PH$_3$ fraction from GaAsP NWs grown at 550 °C (the solid line is a nonlinear model fit (eq 2) to the data points).

measured from the SEM images and the average NW length is indicated on each image. The lower panel in each image is a representative single wire image.

The figure shows that the wires are in all cases straight and untapered. It can also be noted from Figure 2b−d that some nanowires with much smaller diameter can be seen connected

to 80 nm dimeter Au seeded NWs. Some larger particles can also be seen in Figure 2d, the sample taken at the same growth temperature but higher V/III ratio. The elemental composition of these particles was analyzed and they were found to be GaAsP particles with varying P content. We believe that a
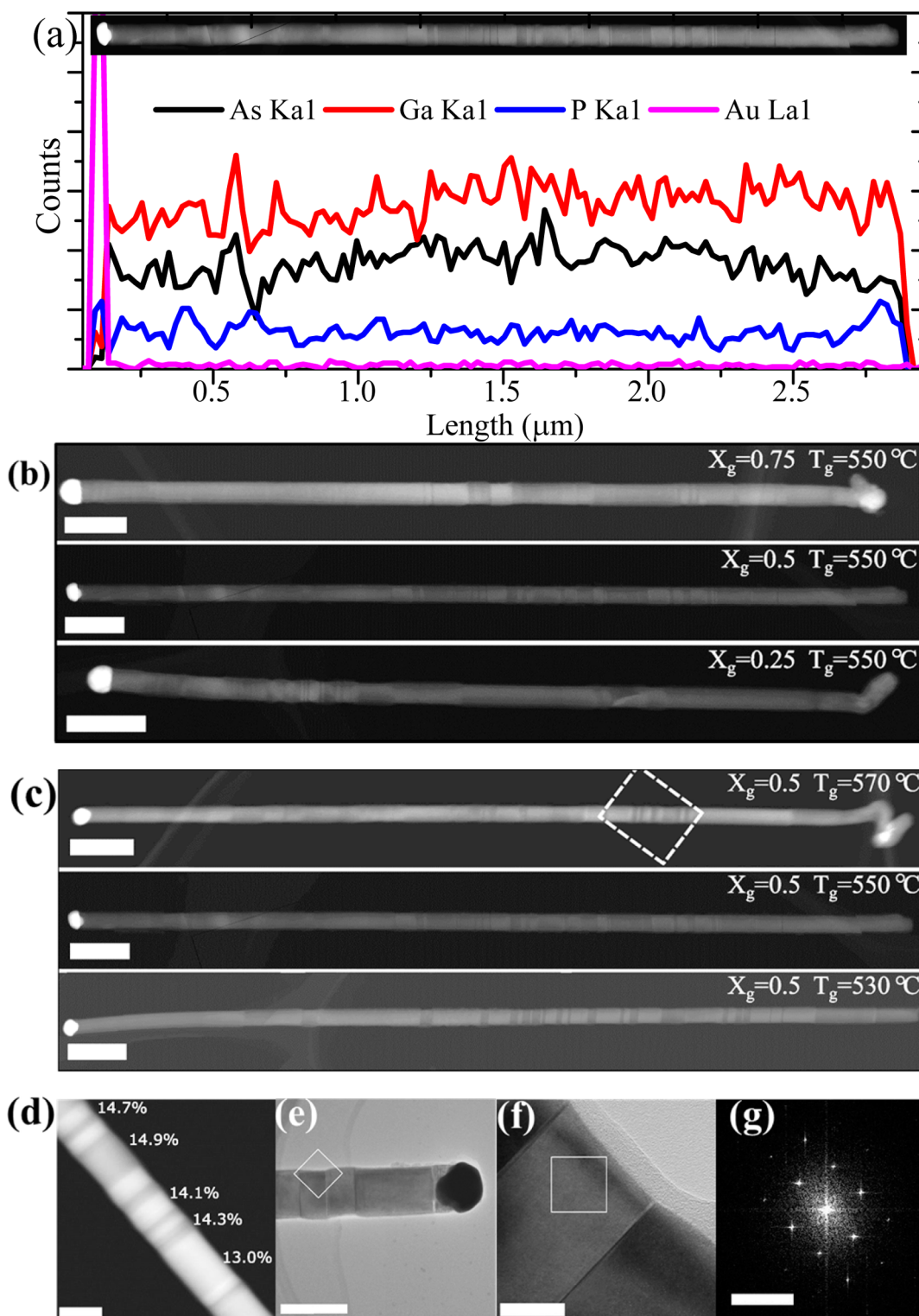
Figure 4. (a) XEDS line scan of a NW grown at $X_g = 0.50$ and growth temperature of 550 °C with inset of STEM-HAADF image of the same wire (see Supporting Information for quantitative XEDS point measurements); the Au seed particle is located at 0 μm. STEM-HAADF images of GaAsP NWs grown (b) at a growth temperature of 550 °C and X_g indicated on each image (c) with $X_g = 0.50$ and growth temperature indicated on each image; scale bars in all images are 200 nm. The dashed square indicates the region analyzed by XEDS and showing a uniform P distribution (shown in atomic percentage) shown in (d). (e) Bright-field TEM image (scale bar 100 nm) showing the twins in a NW grown at 550 °C and $X_g = 0.50$ with a corresponding high-resolution image from the area indicated by the rectangle is shown in (f,g) is FFT of the marked region in (f) (scale bar is 5 nm^{-1}).

systematic study on the effect of V/III and AsH_3/PH_3 ratios should be done to further understand the growth behavior.

Photoluminescence measurements were used to study the optical quality of the NWs and to extract the solid phase ratio
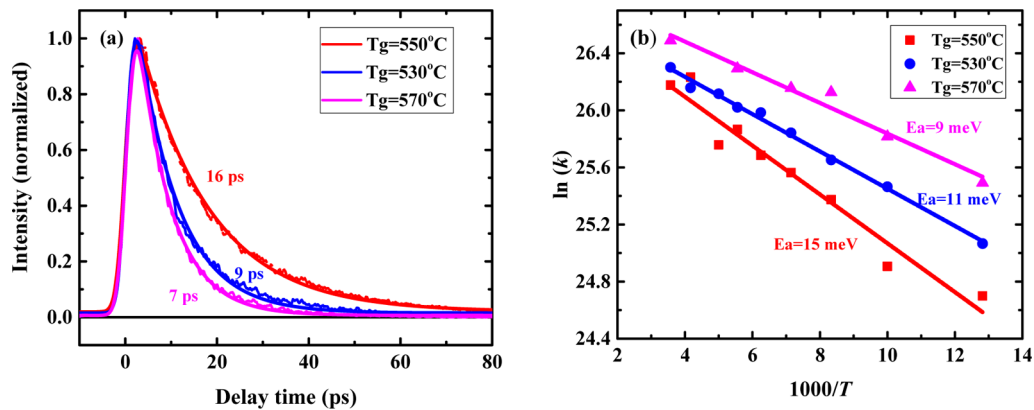
Figure 5. (a) TPRL decay of GaAsP NWs grown with X_g = 0.50 and at growth temperatures of 530, 550, and 570 °C measured at 78 K after photoexcitation at 400 nm. Solid smooth lines are monoexponential fits to the data; (b) temperature-dependent PL decay rates of the three samples. The lines are the linear fits to the data.

of phosphorus, $\left(x = \frac{[P]}{[P] + [As]}\right)$, in GaAs$_{(1-x)}P_x$ from the PL peak energies. Figure 3a shows the low-temperature (4 K) PL spectra from intrinsic GaAs NWs grown at 550 °C and GaAsP NWs grown at 530, 550, and 570 °C with X_g = 0.25, 0.50, and 0.75 at each temperature. Figure 3b shows the dependence of the extracted band gap energies on the input PH$_3$ fraction (X_g). For the nanowires grown with X_g = 0.25 and 0.75, the band gap energies appear to be more or less independent of the growth temperature, that is, the wires grown at the three growth temperatures emit at the same energy of 1.61 and 2.06 eV (at 4 K), respectively. The 1.6 and 2.06 eV band gap energies correspond to x = 0.08 and 0.43, respectively, extracted from PL assuming a direct-gap bowing parameter 0.19 eV.[21] However, for NWs grown with X_g = 0.50 the band gap energy increased with the growth temperature, that is, band gap energies 1.78, 1.80, and 1.85 eV (from low-temperature PL) and 1.71, 1.73, and 1.77 eV (from RT PL) (Supporting Information, S2) for the NWs grown at 530, 550, and 570 °C, respectively, could be obtained. Note that this range of band gap energies is particularly interesting for dual-junction GaAsP based solar cells on silicon.[22] The observed increase in P content with temperature at X_g = 0.50 is attributed to the kinetically controlled PH$_3$ decomposition.[23]

Regardless of the growth temperature used in the study, the P content in the NWs increases with the PH$_3$ fraction in the gas phase. However, the increase is not linear and the fraction of P incorporated in the solid is different from the PH$_3$ fraction in the investigated range growth parameters. Although it is not fully investigated here for Aerotaxy, this tendency has been observed in MOCVD growth of GaAsP thin films and NWs and could be attributed to the difference in the sticking coefficients and arrival rates of arsenic and phosphorus.[24,25] Arsenic adatoms have a larger sticking coefficient and hence a longer lifetime on the catalyst and the NW surface that increases their chance of meeting the Ga atom and incorporating in the lattice.[26−28]

As can be seen from the PL spectra in Figure 3a and discussed above, the P content in the nanowires is strongly related to the input gas phase ratio. To understand this further, x was estimated from the PL spectra of the NWs grown at 550 °C and plotted against the input PH$_3$ fraction in Figure 3b. The squares and the line in the graph represent the experimental data points and nonlinear fit of the data points in that region (0 ≤ X_g ≤ 0.75), respectively. As defined earlier, the input PH$_3$

fraction, X_g is the ratio of input gas fluxes, therefore, the P content in the nanowires, $x = \frac{[P]}{[P] + [As]}$ can be redefined as in eq 1

$$x = \frac{\gamma X_g}{\gamma X_g + \beta(1 - X_g)} \qquad (1)$$

where γ and β are the incorporation rate coefficients of P and As, respectively. The incorporation ratio of P to As can then be defined as $\gamma/\beta = \alpha$ and the P content in the wires can be rewritten as in eq 2

$$x = \frac{\alpha X_g}{1 + X_g(\alpha - 1)} \qquad (2)$$

As can be seen in Figure 3b, eq 2 fits very well to the experimental data when α = 0.26. This fitting helps to link the input PH$_3$ gas flux to the P content in the nanowires for 0 ≤ X_g ≤ 0.75, and it is useful in the control of the GaAsP nanowire composition in Aerotaxy. The obtained value of α indicates in Aerotaxy growth of GaAsP NWs at a given experimental conditions that As incorporates more (about 4 times higher in the this case) than P, as also observed in GaAsP NWs grown in MOCVD.[17,29] This is also similar to the planar epitaxial growth of GaAsP layers grown by MOCVD[23,30,25] and gas and solid source MBE.[26,27,31] For planar epitaxial growth of GaAsP in MOCVD, Samuelson et al.[25] showed a temperature-dependent incorporation rate ratio, α (0.077 ≤ α ≤ 0.75) in the temperature range of 650−850 °C and 0 ≤ X_g ≤ 1. This means that the value of α obtained for Aerotaxy at a growth temperature of 550 °C for GaAsP NWs in Aerotaxy is larger than for the thin film growth in MOCVD. Apart from the inherent difference between Aerotaxy and MOCVD[32] and the difference in growth mechanism between NWs and thin films, which might be attributed to this difference in the incorporation rate, the Au catalyst in the NW growth could also be responsible for enhanced P (and As) incorporation by enhancing the decomposition of PH$_3$ as shown by Wen et al.[17] by simultaneous growth of GaAsP NWs and thin film on GaAs in MOCVD.

X-ray energy dispersive spectroscopy (XEDS) operating in scanning-mode TEM is used to further study the distribution of P in the nanowires. A total of 5−10 nanowires from each sample were analyzed, and in each case the P content along the wire length is found to be uniform within the accuracy of the

method. Figure 4 a shows an integrated XEDS line scan from a GaAsP NW grown at 550 °C and X_g = 0.50 (see also Supporting Information S3). The average P content is consistent with the PL measurement. Structural studies performed by HR-TEM reveal that, regardless of the variations in X_g and growth temperature, NWs from all samples are pure zincblende (ZB) crystal structure (Figure 4b,c). Stacking faults in the form of twinning were found but no other polytypes observed. Alternating dark and bright contrast is seen in the STEM-HAADF images of all wires. XEDS spot analyses were performed within a region indicated by a dashed rectangle in Figure 4c. The analysis shows no compositional difference for any of the elements. Full quantification for P is shown in Figure 4d. Hence, we conclude that this contrast is due to twin segments resulting in a difference in projected thickness. The HRTEM-image and its fast Fourier transform (FFT), Figure 4f,g, reveal a pure ZB crystal structure mirrored at the twin planes, which is valid for all observed wires.

The GaAsP NWs grown with X_g = 0.50 and at the three temperatures (530, 550, and 570 °C) were further characterized by low-temperature (78 K) TRPL spectroscopy at an excitation fluency of 1.3×10^{13} photons cm^{-2} pulse^{-11}. Figure 5 a shows the TRPL decays of the three samples. The decay curves for all the samples fit well with single exponential functions, suggesting that the decays are dominated by charge trapping.[33] This was further verified by excitation power dependent PL decay lifetime at 78 K where the carrier lifetime increases with the increase of the excitation power (Supporting Information, S4). The NWs grown at 550 °C show a longer lifetime, 16 ps, than the NWs grown at 530 °C, 9 ps, and at 570 °C, 7 ps, respectively. To study the details of the charge radiative recombination processes in these samples, we measured the temperature-dependent TRPL. We observe that PL decays faster with increasing temperature (Supporting Information, S4) and that the temperature dependences fit very well with a thermally activated charge trapping model.[34,35] Thus, the activation energies of the carrier trapping were determined from the Arrhenius plot by fitting eq 3

$$\ln(k) = \frac{E_a}{k_B}\left(\frac{1}{T}\right) + \ln(A) \tag{3}$$

where k_B is the Boltzmann constant, E_a is the activation energy, and A is the pre-exponential factor. The activation energy can then be given by the slope of the linear fit to the data in Figure 5 b. We obtained activation energies of 11, 15, and 9 meV for NWs grown at 530, 550, and 570 °C, respectively. This indicates that charges are more likely to be trapped for the NWs grown at 530 and 570 °C. Carrier trapping can be induced by, for example, bulk defects such as stacking faults, alloy fluctuations, or surface traps. Because the diameters of NWs grown at 530, 550, and 570 °C are similar, we would expect similar PL decay of the NWs if the charge trapping are dominated by the surface traps. Therefore, carrier trapping is most probably induced by the bulk defects. From the steady-state PL in Figure 3a, it can be seen that the spectrum from the NWs grown at 570 °C and with X_g = 0.50 is broad with a shoulder at 1.81 eV. From our TEM studies, we find that the wires have bulk/twinning defects, which may act as traps and affect the shape of the PL spectra and also quench the PL intensity.

In summary, we demonstrate for the first time, using the Aerotaxy growth mode, the growth of GaAsP nanowires with band gaps ranging from 1.42 to 1.90 eV (at 300 K) by Aerotaxy, which is an essential step toward low-cost high-efficiency tandem nanowire solar cells on silicon. Both the input gas fraction of PH_3 and growth temperature are shown to affect the phosphorus composition/bandgap energy of the NWs. For the range of growth parameters investigated in this work, the wires are untapered and pure zinc-blende and with low density of twinning defects. GaAsP NWs with band gap of 1.71−1.77 eV (at room temperature), ideal band gap energies for dual-junction solar cells on silicon, could be grown with PH_3/AsH_3 ratio of 1:1 and at a growth temperature in the range between 530 and 570 °C. The 550 °C growth temperature at that ratio resulted in a better optical quality NWs confirmed by steady-state and time-resolved photoluminescence measurements. Further experiments with a special focus on the effect of growth parameters in combination with in situ TEM studies[36] will help to gain more understanding on the growth behavior and produce high quality NWs for device applications.

■ ASSOCIATED CONTENT

ⓢ Supporting Information

The Supporting Information is available free of charge on the ACS Publications website at DOI: 10.1021/acs.nano-lett.6b02367.

> Additional SEM images, room-temperature PL spectrum, XEDS line scans, and low-temperature TRPL spectrum of GaAsP NWs (PDF)

■ AUTHOR INFORMATION

Corresponding Authors
*E-mail: (W.M.) wondwosen.metaferia@ftf.lth.se.
*E-mail: (M.H.M.) martin.magnusson@ftf.lth.se.

Author Contributions

The manuscript was written with contributions from all authors. All authors have given approval to the final version of the manuscript.

Notes

The authors declare no competing financial interest.

■ ACKNOWLEDGMENTS

■ REFERENCES

(1) Samuelson, L.; Thelander, C.; Björk, M. T.; Borgström, M.; Deppert, K.; Dick, K. A.; Hansen, A. E.; Mårtensson, T.; Panev, N.; Persson, A. I.; Seifert, W.; Sköld, N.; Larsson, M. W.; Wallenberg, L. R. *Phys. E* **2004**, *25* (2−3), 313−318.

(2) Berg, A.; Yazdi, S.; Nowzari, A.; Storm, K.; Jain, V.; Vainorius, N.; Samuelson, L.; Wagner, J. B.; Borgström, M. T. *Nano Lett.* **2016**, *16* (1), 656−662.

(3) Åberg, I.; Vescovi, G.; Asoli, D.; Naseem, U.; Gilboy, J. P.; Sundvall, C.; Dahlgren, A.; Svensson, K. E.; Anttu, N.; Björk, M. T.; Samuelson, L. *IEEE J. Photovolt.* **2016**, *6* (1), 185−190.

(4) Wallentin, J.; Anttu, N.; Asoli, D.; Huffman, M.; Åberg, I.; Magnusson, M. H.; Siefer, G.; Fuss-Kailuweit, P.; Dimroth, F.; Witzigmann, B.; Xu, H. Q.; Samuelson, L.; Deppert, K.; Borgström, M. T. *Science* **2013**, *339* (6123), 1057−1060.

(5) Zhu, H.; Fu, Y.; Meng, F.; Wu, X.; Gong, Z.; Ding, Q.; Gustafsson, M. V.; Trinh, M. T.; Jin, S.; Zhu, X.-Y. *Nat. Mater.* **2015**, *14* (6), 636−642.

(6) Ielmini, D.; Cagli, C.; Nardi, F.; Zhang, Y. *J. Phys. D: Appl. Phys.* **2013**, *46* (7), 074006.

(7) Seifert, W.; Borgström, M.; Deppert, K.; Dick, K. A.; Johansson, J.; Larsson, M. W.; Mårtensson, T.; Sköld, N.; Patrik, T.; Svensson, C.; Wacaser, B. A.; Reine Wallenberg, L.; Samuelson, L. *J. Cryst. Growth* **2004**, *272* (1−4), 211−220.

(8) Caroff, P.; Wagner, J. B.; Dick, K. A.; Nilsson, H. A.; Jeppsson, M.; Deppert, K.; Samuelson, L.; Wallenberg, L. R.; Wernersson, L.-E. *Small* **2008**, *4* (7), 878−882.

(9) Borgström, M.; Deppert, K.; Samuelson, L.; Seifert, W. *J. Cryst. Growth* **2004**, *260* (1−2), 18−22.

(10) Fortuna, S. A.; Wen, J.; Chun, I. S.; Li, X. *Nano Lett.* **2008**, *8* (12), 4421−4427.

(11) Tsivion, D.; Schvartzman, M.; Popovitz-Biro, R.; Huth, P.; von Joselevich, E. *Science* **2011**, *333* (6045), 1003−1007.

(12) La, R.; Pan, J. L.; Bastiman, F.; Tu, C. W. *J. Vac. Sci. Technol. B* **2016**, *34* (2), 02L108.

(13) Ohlsson, B. J.; Björk, M. T.; Magnusson, M. H.; Deppert, K.; Samuelson, L.; Wallenberg, L. R. *Appl. Phys. Lett.* **2001**, *79* (20), 3335−3337.

(14) Heurlin, M.; Magnusson, M. H.; Lindgren, D.; Ek, M.; Wallenberg, L. R.; Deppert, K.; Samuelson, L. *Nature* **2012**, *492* (7427), 90−94.

(15) Yang, F.; Messing, M. E.; Mergenthaler, K.; Ghasemi, M.; Johansson, J.; Wallenberg, L. R.; Pistol, M.-E.; Deppert, K.; Samuelson, L.; Magnusson, M. H. *J. Cryst. Growth* **2015**, *414*, 181−186.

(16) Joyce, H. J.; Gao, Q.; Tan, H. H.; Jagadish, C.; Kim, Y.; Fickenscher, M. A.; Perera, S.; Hoang, T. B.; Smith, L. M.; Jackson, H. E.; Yarrison-Rice, J. M.; Zhang, X.; Zou, J. *Nano Lett.* **2009**, *9* (2), 695−701.

(17) Sun, W.; Huang, Y.; Guo, Y.; Liao, Z. M.; Gao, Q.; Tan, H. H.; Jagadish, C.; Liao, X. Z.; Zou, J. *J. Mater. Chem. C* **2015**, *3* (8), 1745−1750.

(18) Magnusson, M. H.; Deppert, K.; Malm, J.-O.; Bovin, J.-O.; Samuelson, L. *J. Nanopart. Res.* **1999**, *1* (2), 243−251.

(19) Scheibel, H. G.; Porstendörfer, J. *J. Aerosol Sci.* **1983**, *14* (2), 113−126.

(20) Wacaser, B. A.; Dick, K. A.; Johansson, J.; Borgström, M. T.; Deppert, K.; Samuelson, L. *Adv. Mater.* **2009**, *21* (2), 153−165.

(21) Vurgaftman, I.; Meyer, J. R.; Ram-Mohan, L. R. *J. Appl. Phys.* **2001**, *89* (11), 5815−5875.

(22) LaPierre, R. R. *J. Appl. Phys.* **2011**, *110* (1), 014310.

(23) Smeets, E. T. J. M. *J. Cryst. Growth* **1987**, *82* (3), 385−395.

(24) *The Handbook of Surface Imaging and Visualization*; https://www.crcpress.com/The-Handbook-of-Surface-Imaging-and-Visualization/Hubbard/p/book/9780849389115 (accessed Jun 1, 2016).

(25) Samuelson, L.; Omling, P.; Titze, H.; Grimmeiss, H. *J. Phys. Colloq.* **1982**, *43* (C5), C5-323−C5−338.

(26) Shu-Dong, W.; Li-Wei, G.; Wen-Xin, W.; Zhi-Hua, L.; Ping-Juan, N.; Qi, H.; Jun-Ming, Z. *Chin. Phys. Lett.* **2005**, *22* (4), 960.

(27) Hou, H. Q.; Liang, B. W.; Chin, T. P.; Tu, C. W. *Appl. Phys. Lett.* **1991**, *59* (3), 292−294.

(28) Matsushima, Y.; Gonda, S. *Jpn. J. Appl. Phys.* **1976**, *15* (11), 2093−2101.

(29) Im, H. S.; Jung, C. S.; Park, K.; Jang, D. M.; Lim, Y. R.; Park, J. *J. Phys. Chem. C* **2014**, *118* (8), 4546−4552.

(30) Seki, H.; Koukitu, A. *J. Cryst. Growth* **1986**, *74* (1), 172−180.

(31) LaPierre, R. R.; Robinson, B. J.; Thompson, D. A. *J. Appl. Phys.* **1996**, *79* (6), 3021−3027.

(32) *Growth of Semiconductor Nanowires for Solar Cell Applications*; https://lup.lub.lu.se/search/publication/8084551 (accessed Mar 21, 2016).

(33) Zhang, Y.; Aagesen, M.; Holm, J. V.; Jørgensen, H. I.; Wu, J.; Liu, H. *Nano Lett.* **2013**, *13* (8), 3897−3902.

(34) Titova, L. V.; Hoang, T. B.; Jackson, H. E.; Smith, L. M.; Yarrison-Rice, J. M.; Kim, Y.; Joyce, H. J.; Tan, H. H.; Jagadish, C. *Appl. Phys. Lett.* **2006**, *89* (17), 173126.

(35) Hsiao, C.-L.; Hsu, H.-C.; Chen, L.-C.; Wu, C.-T.; Chen, C.-W.; Chen, M.; Tu, L.-W.; Chen, K.-H. *Appl. Phys. Lett.* **2007**, *91* (18), 181912.

(36) Jacobsson, D.; Panciera, F.; Tersoff, J.; Reuter, M. C.; Lehmann, S.; Hofmann, S.; Dick, K. A.; Ross, F. M. *Nature* **2016**, *531* (7594), 317−322.